



On accounting for preferred crystallite orientations in determination of average elastic strain by diffraction

A. Morawiec

J. Appl. Cryst. (2018). **51**, 148–156



IUCr Journals
CRYSTALLOGRAPHY JOURNALS ONLINE

Copyright © International Union of Crystallography

Author(s) of this paper may load this reprint on their own web site or institutional repository provided that this cover page is retained. Republication of this article or its storage in electronic databases other than as specified above is not permitted without prior permission in writing from the IUCr.

For further information see <http://journals.iucr.org/services/authorrights.html>

On accounting for preferred crystallite orientations in determination of average elastic strain by diffraction

A. Morawiec*

Polish Academy of Sciences, Institute of Metallurgy and Materials Science, Reymonta 25, 30-059 Krakow, Poland.

*Correspondence e-mail: nmmorawi@cyf-kr.edu.pl

Received 1 August 2017

Accepted 2 January 2018

Edited by G. Kostorz, ETH Zurich, Switzerland

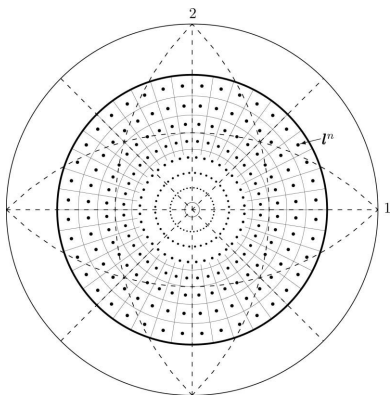
Keywords: polycrystalline materials; elastic anisotropy; crystal lattices; X-ray diffraction; crystallographic texture.

Standard diffraction-based measurements of elastic strains in polycrystalline materials rely on shifts of Bragg peaks. Measurement results are usually given in the form of a single tensor assumed to represent the average stress in the material, but the question about the true relationship between the tensor and the average stress generally goes without notice. This paper describes a novel procedure for analysis of data obtained from such measurements. It is applicable in cases when spatial correlations in the material are ignored and statistical information about the polycrystalline specimen is limited to texture-related intensity pole figures and strain pole figures. A tensor closest to auxiliary strain tensors linked to the results of measurements in particular specimen directions is considered to represent the strain state. This tensor is shown to be a good approximation of the average strain tensor. A closed-form expression allowing for its direct computation from experimental pole figures is given. The performance of the procedure is illustrated using simulated data.

1. Introduction

Stresses in polycrystalline materials, in particular residual stresses present despite the absence of external loads, are frequently determined using X-ray or neutron diffraction techniques. A typical measurement of stresses of the first kind relies on determining shifts of Bragg peaks for various directions of the scattering vector with respect to the specimen. The shifts are directly related to the average distances between lattice planes perpendicular to the scattering vector, and the distances are a basis for determining the stresses (Macher-auch, 1966; Noyan & Cohen, 1987). In the simplest approach, stress is calculated from the slope of a line fitted to points representing measured interplanar spacings *versus* $\sin^2 \psi$, where ψ is the angle between the scattering vector and the normal to the specimen surface.

Measurement results are presented as selected components of a tensor tacitly assumed to represent the average stress in the material. However, despite the apparent simplicity of this approach, the issue of the equality between the measured stress tensor and the average stress tensor is complex, and it is usually left unconsidered (Noyan & Cohen, 1987). Computing a single tensor representing the stresses from measured lattice strains requires a grain interaction model. In general, such models are formally described by infinite perturbation series with terms involving non-local integral operators and spatial correlations (see *e.g.* Beran & McCoy, 1970; Kröner, 1986; and references therein). In practice, under the assumption of random spatial correlations, simple local approximations are used, and the operators are reduced to ordinary tensors. With



such a local approximation, differences in microstructures are neglected, and effective properties are influenced only by crystallographic textures. In other words, only orientation density functions are needed for averaging. Even with this approximation, various averaging methods can be used, from the simplest Voigt and Reuss averages (based on the assumptions of constant strain and stress, respectively) to more sophisticated schemes conforming with the assumption of local approximation (Bollenrath *et al.*, 1967; Dölle, 1979; de Wit, 1997). In the conventional stress determination, the Reuss model is usually assumed. More complex models have also been considered (see *e.g.* van Leeuwen *et al.*, 1999; Leoni *et al.*, 2001; Liu *et al.*, 2010), but in most analyses spatial correlations are ignored.

To avoid choosing the averaging scheme, a simpler problem is discussed below: instead of determining the stress tensor, only the computation of a representative strain tensor is considered. Thus, within the local approximation, the question is about the relationship between the measured constant strain tensor, denoted below by ε^M , and the average strain $\langle \varepsilon \rangle$ of the crystal lattice, or how to process strain measurement data in order to get ε^M close to $\langle \varepsilon \rangle$.

The tensor ε^M is determined by a linear optimization problem. Abandoning the simplistic $\sin^2 \psi$ method in favor of a more inclusive fitting was advocated by Ortner (2008, 2009). The procedure described below is a generalization of the method proposed by Winholtz & Cohen (1988) to the case of non-random orientation distribution. In the presence of a strong crystallographic texture, the fitting gives ε^M close to the average strain only if the strain measurements in particular directions are weighted by the radiation intensities in these directions, *i.e.* by the corresponding texture-related pole figures. A closed-form expression for ε^M involves experimental intensity pole figures and strain pole figures.

The paper begins with basics about the change of the scattering vector caused by straining a crystal and about the representation of crystallite orientations. Next, a procedure for obtaining ε^M is described for a theoretical case. So defined, ε^M is shown to be equal to $\langle \varepsilon \rangle$ if certain undetectable strains are ignored. Then, it is demonstrated that some experimentally accessible data can be processed in an analogous way. At the outset, the case of a single reflection is dealt with. The generalization to multiple reflections is given later on. Finally, the new approach is applied to special textures and to some simulated data. It is assumed throughout the paper that the diffraction data are collected from a representative volume of a statistically homogeneous polycrystalline material. The reference lattice parameters are assumed to be known, and the crystal structure is assumed to have a center of inversion.

2. Basics

2.1. Shift of a Bragg peak

Let I denote the identity tensor, *i.e.* $I_{ij} = \delta_{ij}$, where δ is the Kronecker delta. If a small deformation of a crystal is

described by the deformation gradient tensor $I + \varepsilon$, then a vector \mathbf{h} of the crystal reciprocal lattice is transformed to

$$\mathbf{h}' = (I - \varepsilon)\mathbf{h}. \quad (1)$$

Let \mathbf{l}^c denote the unit vector along \mathbf{h} ; in this context, \mathbf{l}^c is meant to be referred to the crystal reference frame. The same vector will be denoted by \mathbf{l} when referred to the specimen reference frame. The squared ratio of magnitudes of \mathbf{h}' and \mathbf{h} can be expressed as $\mathbf{h}'^2/\mathbf{h}^2 \simeq 1 - 2\varepsilon_{ij}^c l_i^c l_j^c$, where ε_{ij}^c are components of ε in the crystal coordinate system. Under the assumption that the magnitudes of close scattering vectors are similar, the magnitude of \mathbf{h}' is measured in the proximate direction of \mathbf{h} . The (single-crystal) strain

$$e^{sc} = \varepsilon_{ij}^c l_i^c l_j^c \quad (2)$$

is directly linked to the change of the lattice plane spacing and the shift of the Bragg peak:

$$e^{sc} \simeq \frac{1}{2} \left(1 - \frac{d'^2}{d^2} \right) \simeq \frac{d' - d}{d} \simeq -(\theta' - \theta) \cot \theta, \quad (3)$$

where $d = 1/|\mathbf{h}|$ and $d' = 1/|\mathbf{h}'|$ are interplanar spacings, and θ and θ' are Bragg angles corresponding to \mathbf{h} and \mathbf{h}' , respectively.

2.2. Crystallite orientation

Crystallite orientations are described here using standard conventions of texture analysis (Bunge, 1982; Morawiec, 2004). An orientation is determined by a special orthogonal matrix g or by Euler angles $\varphi_1, \phi, \varphi_2$, and there is a relationship between the angles and the matrix $g = \Phi(\varphi_1, \phi, \varphi_2)$. The formula for Φ can be found in numerous articles and books (Bunge, 1982; Morawiec, 2004); for completeness it is also listed in Appendix A. The matrix g links vector components in Cartesian reference frames attached to the crystal and the specimen. In particular, with l_i being components of \mathbf{l} in the specimen coordinate system, one has

$$l_i^c = g_{ij} l_j. \quad (4)$$

The measurement of strain in the direction \mathbf{l} with the use of the reflection $\mathbf{h} \propto \mathbf{l}^c$ involves crystallites with orientations satisfying the above relationship.

By convention, the direction of the scattering vector is also described by spherical angles ψ (polar angle in $[0, \pi]$) and φ (azimuth), *i.e.* $[l_1, l_2, l_3] = [\cos \varphi \sin \psi, \sin \varphi \sin \psi, \cos \psi]$. Similarly, it can be expressed by spherical angles α and β in the crystal reference frame, *i.e.* $[l_1^c, l_2^c, l_3^c] = [\cos \beta \sin \alpha, \sin \beta \sin \alpha, \cos \alpha]$. The matrix representing the rotation transforming l_i to l_i^c can be decomposed into the product

$$g = g^c(\mathbf{l}^c) g^z(\gamma) g^s(\mathbf{l}), \quad (5)$$

where $g^c(\mathbf{l}^c) = \Phi(0, \alpha, \pi/2 - \beta)$, $g^z(\gamma) = \Phi(0, 0, \gamma)$ and $g^s(\mathbf{l}) = \Phi(\pi/2 + \varphi, \psi, 0)$. One can easily verify that $g_{ij}^s l_j = \delta_{i3}$, $g_{ij}^z \delta_{j3} = \delta_{i3}$ and $g_{ij}^c \delta_{j3} = l_i^c$, *i.e.* equation (4) is satisfied (Morawiec & Pospiech, 1989). In the above decomposition, \mathbf{l}^c is fixed by the choice of diffracted reflection. The crucial point is to notice that, with a given reflection, the crystal orientation can be parametrized by the angles ψ, φ, γ , or briefly, by the pair (\mathbf{l}, γ) .

An orientation density function (ODF) will be denoted by $f = f(g)$. Assuming a particular reflection is considered, f can be seen as a function of (\mathbf{l}, γ) , *i.e.* by abuse of notation, $f = f(\mathbf{l}, \gamma)$. By definition, the ODF is normalized to one, *i.e.* $\int_g f(g) = 1 = \int_{\mathbf{l}} \int_{\gamma} f(\mathbf{l}, \gamma)$, where the abbreviated symbol \int_x denotes integration over the complete domain of x . The domain of g consists of all special orthogonal matrices, and the domains of \mathbf{l} and γ are the unit sphere and the unit circle, respectively. The explicit forms of \int_{γ} and $\int_{\mathbf{l}}$ are $(2\pi)^{-1} \int_0^{2\pi} d\gamma$ and $(4\pi)^{-1} \int_0^{2\pi} d\varphi \int_0^{\pi} d\psi \sin \psi$, respectively, and \int_g can be expressed *via* $\int_{\mathbf{l}} \int_{\gamma}$.

For a given reflection, the integral of $f(\mathbf{l}, \gamma)$ over γ represents an unreduced (this term is used in literature on reproducibility of ODFs from pole figures; see *e.g.* Matthies & Wenk, 1985) pole figure p at \mathbf{l} , *i.e.*

$$\int_{\gamma} f(\mathbf{l}, \gamma) = p(\mathbf{l}). \quad (6)$$

This definition implies that $\int_{\mathbf{l}} p(\mathbf{l}) = 1$. For simplicity, it is assumed below that $p(\mathbf{l}) \neq 0$ for all \mathbf{l} . The value of the pole figure p at \mathbf{l} represents the frequency of occurrence of crystallite orientations with the scattering vector along \mathbf{l} . For these particular crystallites, *i.e.* for a given \mathbf{l} , the frequency of occurrence of crystallite orientations with various γ angles will be denoted by

$$q_1(\gamma) = f(\mathbf{l}, \gamma)/p(\mathbf{l}). \quad (7)$$

Clearly, also the functions q_1 are normalized to one: $\int_{\gamma} q_1(\gamma) = 1$.

3. Strain pole figures and average strain

With a given vector \mathbf{l} and variable angle γ , only crystallites with orientations (\mathbf{l}, γ) contribute their strains e^{sc} to the polycrystalline strain $e(\mathbf{l})$. The latter quantity is the average of $e^{\text{sc}}(\mathbf{l}, \gamma)$ weighted by the frequency of occurrence $q_1(\gamma)$ of orientations along γ :

$$e(\mathbf{l}) = \int_{\gamma} q_1(\gamma) e^{\text{sc}}(\mathbf{l}, \gamma) = \int_{\gamma} q_1(\gamma) \varepsilon_{ij}(\mathbf{l}, \gamma) l_i l_j = \varepsilon_{ij}^t(\mathbf{l}) l_i l_j, \quad (8)$$

where ε_{ij} and ε_{ij}^t are components of ε and

$$\varepsilon^t(\mathbf{l}) = \int_{\gamma} q_1(\gamma) \varepsilon(\mathbf{l}, \gamma) \quad (9)$$

in the specimen reference system (*cf.* Van Houtte & De Buyser, 1993). The tensor $\varepsilon^t(\mathbf{l})$ is the average of the actual strain $\varepsilon = \varepsilon(\mathbf{l}, \gamma)$ in crystallites contributing to e at \mathbf{l} . The function $e = e(\mathbf{l})$ represents an (unreduced) strain pole figure.

The strain pole figure is the basis for determining the strain tensor ε^M . Similarly to the average strain $\langle \varepsilon \rangle = \int_g f(g) \varepsilon(g)$, the tensor ε^M is assumed to describe the state of the sample as a whole. The task is to devise a method of processing $e(\mathbf{l})$ so the resulting ε^M would come close to the actual strain in the material and to $\langle \varepsilon \rangle$. Here, the tensor ε^M is assumed to be as close as possible to the function $\varepsilon^m = \varepsilon^m(\mathbf{l})$ linked to known $e(\mathbf{l})$ in the same way as $\varepsilon^t(\mathbf{l})$ [see equation (8)]. Formally, ε^M is defined as

$$\varepsilon^M = \arg_{\varepsilon^X} \min_{\varepsilon^X, \varepsilon^m} \int_{\mathbf{l}} p(\mathbf{l}) \|\varepsilon^X - \varepsilon^m(\mathbf{l})\|^2 \quad (10)$$

subject to $\varepsilon_{ij}^m(\mathbf{l}) l_i l_j = e(\mathbf{l})$, where $\|\cdot\|$ denotes the Frobenius norm ($\|x\|^2 = x_{ij}x_{ij}$). The weighting by the pole figure p is needed to account for different populations of crystallites contributing to ε^m at particular \mathbf{l} and, consequently, for differences in their influence on the strain state.

It remains to get a closed-form expression for ε^M , and to investigate the link between ε^M and $\langle \varepsilon \rangle$. With $\mu(\mathbf{l})$ being a Lagrange multiplier, conditions for extrema of the ε^X - and ε^m -dependent integral $\int_{\mathbf{l}} p(\mathbf{l}) \|\varepsilon^X - \varepsilon^m(\mathbf{l})\|^2 + 2 \int_{\mathbf{l}} p(\mathbf{l}) \mu(\mathbf{l}) \times [\varepsilon_{ij}^m(\mathbf{l}) l_i l_j - e(\mathbf{l})]$ have the form

$$\varepsilon^M = \int_{\mathbf{l}} p(\mathbf{l}) \varepsilon^m(\mathbf{l}) \quad \text{and} \quad \varepsilon_{ij}^m(\mathbf{l}) = \varepsilon_{ij}^M + \mu(\mathbf{l}) l_i l_j, \quad (11)$$

where ε^X was replaced by ε^M . With the condition $\varepsilon_{ij}^m(\mathbf{l}) l_i l_j = e(\mathbf{l})$, the second of equations (11) gives $\mu(\mathbf{l}) = e(\mathbf{l}) - \varepsilon_{ij}^M l_i l_j$ and

$$\varepsilon_{ij}^m(\mathbf{l}) = \varepsilon_{ij}^M + [e(\mathbf{l}) - \varepsilon_{kl}^M l_k l_l] l_i l_j. \quad (12)$$

Replacement of $\varepsilon^m(\mathbf{l})$ in the first of equations (11) by the above expression leads to $\varepsilon_{ij} = A_{ijkl}^C \varepsilon_{kl}^M$, where

$$\varepsilon_{ij} = \int_{\mathbf{l}} p(\mathbf{l}) e(\mathbf{l}) l_i l_j \quad \text{and} \quad A_{ijkl}^C = \int_{\mathbf{l}} p(\mathbf{l}) l_i l_j l_k l_l. \quad (13)$$

Hence, the sought strain tensor ε^M of equation (5) is given by

$$\varepsilon^M = A^S \varepsilon. \quad (14)$$

Here, A^S is the inverse of A^C in the same sense as a compliance tensor is the inverse of the corresponding stiffness tensor, *i.e.* $A^C A^S = I^{(4)}$, where $I_{ijkl}^{(4)} = (\delta_{ik} \delta_{jl} + \delta_{il} \delta_{jk})/2$. If A^C happens to be singular, A^S is its pseudoinverse (Ben-Israel & Greville, 2003). Note that ε^M also solves the simpler optimization problem

$$\varepsilon^M = \arg \min_{\varepsilon^X} \int_{\mathbf{l}} p(\mathbf{l}) [\varepsilon_{ij}^X l_i l_j - e(\mathbf{l})]^2, \quad (15)$$

which is a generalization of that described by Winholtz & Cohen (1988) to cases with non-uniform orientation distributions.¹ The procedure based on the more complex equation (10) additionally provides formula (12) for ε^m . The auxiliary tensor $\varepsilon^m(\mathbf{l})$ has a simple interpretation as an approximation of the actual $\varepsilon^t(\mathbf{l})$. The latter can be expressed as $\varepsilon^t(\mathbf{l}) = \varepsilon^m(\mathbf{l}) + \varepsilon^d(\mathbf{l})$, where $\varepsilon^d(\mathbf{l})$ has no impact on $e(\mathbf{l})$ [as $\varepsilon_{ij}^d(\mathbf{l}) l_i l_j = 0$] and, consequently, is inaccessible in the measurement by the assumed reflection. Of all ε^t satisfying equations (8) and (9), $\varepsilon^t = \varepsilon^m$ is the closest to the constant ε^M . By the principle of parsimony, if one needs to choose ε^t , the best approach is to take the simplest (closest to constant) tensor ε^m . Thus, ε^m seen as an approximation of the actual ε^t is optimal in the sense that there is no experimental information for indicating a better tensor satisfying equations (8) and (9).

¹ Analogy to the paper of Winholtz & Cohen (1988) is complete with a texture-comprising formula for ‘measured’ stress, $\sigma^M = \arg \min_{\sigma^X} \int_{\mathbf{l}} p(\mathbf{l}) [F_{ij}(\mathbf{l}) \sigma_{ij}^X - e(\mathbf{l})]^2$, where $F_{ij}(\mathbf{l})$ denote the stress factors of Dölle (1979). Similarly to the above expressions for ε^M , one has $\sigma^M = B^S \zeta$, where $\zeta_{ij} = \int_{\mathbf{l}} p(\mathbf{l}) e(\mathbf{l}) F_{ij}(\mathbf{l})$ and B^S is the inverse of $B_{ijkl}^S = \int_{\mathbf{l}} p(\mathbf{l}) F_{ij}(\mathbf{l}) F_{kl}(\mathbf{l})$. With this formulation, one faces the problem of determining the stress factors.

Moreover, the auxiliary ε^m is convenient for showing the link between the average strain and the strain tensor ε^M defined by equation (10). The average $\langle \varepsilon \rangle$ is equal to the integral of ε^t weighted by p :

$$\langle \varepsilon \rangle = \int_g f(g) \varepsilon(g) = \int_{\mathbf{l}} \int_{\gamma} p(\mathbf{l}) q_1(\gamma) \varepsilon(\mathbf{l}, \gamma) = \int_{\mathbf{l}} p(\mathbf{l}) \varepsilon^t(\mathbf{l}), \quad (16)$$

and the first of equations (11) gives

$$\langle \varepsilon \rangle = \varepsilon^M + \int_{\mathbf{l}} p(\mathbf{l}) \varepsilon^d(\mathbf{l}). \quad (17)$$

Generally, the second term is nonzero, and there is an ambiguity in determination of the average strain $\langle \varepsilon \rangle$. If the experimentally inaccessible part of ε^t is neglected ($\varepsilon^d = 0$), one has $\langle \varepsilon \rangle = \varepsilon^M$.

4. Strain from experimental data

The strains $e(+\mathbf{l})$ and $e(-\mathbf{l})$ are generally different. This follows directly from equation (8) and the observation that the integration path (\mathbf{l}, γ) with a fixed \mathbf{l} and variable γ is different from the path $(-\mathbf{l}, \gamma)$. On the other hand, it is important to recall that measurements of strain rely on the geometry of diffraction and the crystal lattice. The latter is always centrosymmetric, and a conventional diffraction-based measurement for a reflection \mathbf{h} is inseparable from that for $-\mathbf{h}$. In real experiments, all crystallites with $+\mathbf{h}$ or $-\mathbf{h}$ along \mathbf{l} contribute to the shift of Bragg peaks measured at \mathbf{l} , and the measured strain equals

$$\tilde{e}(\mathbf{l}) = \frac{e(+\mathbf{l}) + e(-\mathbf{l})}{2} = \tilde{\varepsilon}_{ij}^e(\mathbf{l}) l_i l_j. \quad (18)$$

Thus, the obtainable strain pole figure \tilde{e} is the even component of e . Experimental figures of this type recoded in various research contexts are reported elsewhere (see *e.g.* Maurer *et al.*, 1988; Perlovich *et al.*, 1997; Larsson *et al.*, 2004; Pang *et al.*, 2006; McNelis *et al.*, 2013; Wielewski *et al.*, 2017).

A diffraction-based measurement of texture-related pole figures goes beyond the geometry as it involves peak intensities. However, an experimental pole figure \tilde{p} recorded at \mathbf{l} has contributions from crystallites with orientations g satisfying $\pm l_i^c = g_{ij} l_j$, and thus

$$\tilde{p}(\mathbf{l}) = \frac{p(\mathbf{l}) + p(-\mathbf{l})}{2}, \quad (19)$$

i.e. the measured pole figure \tilde{p} is the even part of p (Matthies, 1979; Matthies & Wenk, 1985).

Let $\tilde{\varepsilon}^M$ denote the strain tensor to be determined from experimental data $\tilde{e}(\mathbf{l})$. This tensor is expected to approximate the function $\tilde{\varepsilon}^m = \tilde{\varepsilon}^m(\mathbf{l})$ linked to known $\tilde{e}(\mathbf{l})$, and similarly to equation (10), one can define it as

$$\tilde{\varepsilon}^M = \arg_{\tilde{\varepsilon}^x} \min_{\tilde{\varepsilon}^x, \tilde{\varepsilon}^m} \int_{\mathbf{l}} \tilde{p}(\mathbf{l}) \|\tilde{\varepsilon}^x - \tilde{\varepsilon}^m(\mathbf{l})\|^2 \quad (20)$$

subject to $\tilde{\varepsilon}_{ij}^m(\mathbf{l}) l_i l_j = \tilde{e}(\mathbf{l})$. Proceeding as in the case of equation (10), one obtains

$$\tilde{\varepsilon}^M = \tilde{A}^S \tilde{\varepsilon}, \quad (21)$$

where \tilde{A}^S is the (pseudo)inverse of \tilde{A}^C , $\tilde{\varepsilon}_{ij} = \int_{\mathbf{l}} \tilde{p}(\mathbf{l}) \tilde{e}(\mathbf{l}) l_i l_j$ and $\tilde{A}_{ijkl}^C = \int_{\mathbf{l}} \tilde{p}(\mathbf{l}) l_i l_j l_k l_l$. However, the analogy breaks down at equation (17). On the one hand

$$\tilde{\varepsilon}^M = \int_{\mathbf{l}} \tilde{p}(\mathbf{l}) \tilde{\varepsilon}^m(\mathbf{l}) \quad (22)$$

and on the other

$$\langle \varepsilon \rangle = \int_{\mathbf{l}} \tilde{p}(\mathbf{l}) \tilde{\varepsilon}^t(\mathbf{l}) + \int_{\mathbf{l}} \hat{p}(\mathbf{l}) \hat{\varepsilon}^t(\mathbf{l}), \quad (23)$$

where $\hat{p} (= p - \tilde{p})$ and $\hat{\varepsilon}^t (= \varepsilon^t - \tilde{\varepsilon}^t)$ denote odd components of p and ε^t , respectively. Thus, $\tilde{\varepsilon}^M$ additionally differs from $\langle \varepsilon \rangle$ by the integral $\int_{\mathbf{l}} \hat{p}(\mathbf{l}) \hat{\varepsilon}^t(\mathbf{l})$. The latter vanishes if one of the functions p or ε^t is even.

If the point group of the crystal contains a proper rotation c such that $c\mathbf{h} = -\mathbf{h}$ then this symmetry operation transforms the integration path (\mathbf{l}, γ) to the path $(-\mathbf{l}, \gamma)$ (Morawiec & Pospiech, 1989), the functions p and e are even, and one has $\tilde{\varepsilon}^M = \varepsilon^M$. The relationship $c\mathbf{h} = -\mathbf{h}$ is true if \mathbf{h} is perpendicular to a twofold axis of symmetry, and many strong reflections of most common structures satisfy this condition. For example, in the case of cubic metals, these are the $hk0$ - and hkh -type reflections.

In conclusion, the evenness of experimentally accessible pole figures complicates the relationship between the tensor $\tilde{\varepsilon}^M$ and the average strain $\langle \varepsilon \rangle$. However, for a reflection \mathbf{h} such that $c\mathbf{h} = -\mathbf{h}$, one gets the strain tensor satisfying $\tilde{\varepsilon}^M = \varepsilon^M$. In what follows, it will be assumed that only such reflections are used, and the tilde will be omitted. The practical importance of the complication caused by evenness of experimental pole figures in cases with high crystal symmetries and weak textures is low, but as in texture analysis (Matthies, 1979; Matthies & Wenk, 1985), being aware of this issue and understanding its impact is essential for interpretation and processing of pole figure data.

5. Using multiple pole figures

If multiple reflections are considered, one needs to add a sum over the reflections in front of the integrals in equations (10) and (15), and the pole figures p and e need an extra index indicating the reflection, *i.e.* one has $p_{\mathbf{h}}$ and $e_{\mathbf{h}}$. In this notation, the final equations (13) take the form

$$\varepsilon_{ij} = \sum_{\mathbf{h}} \int_{\mathbf{l}} p_{\mathbf{h}}(\mathbf{l}) e_{\mathbf{h}}(\mathbf{l}) l_i l_j \quad \text{and} \quad A_{ijkl}^C = \sum_{\mathbf{h}} \int_{\mathbf{l}} p_{\mathbf{h}}(\mathbf{l}) l_i l_j l_k l_l, \quad (24)$$

and as above, the strain tensor ε^M equals $A^S \varepsilon$, where A^S is the (pseudo)inverse of A^C . Analogously to equation (17), one has $\langle \varepsilon \rangle = \varepsilon^M +$ an indeterminable part which is an arithmetic mean of $\int_{\mathbf{l}} p_{\mathbf{h}}(\mathbf{l}) \varepsilon_{\mathbf{h}}^d(\mathbf{l})$ over the reflections. The strain tensors determined from individual reflections are based on different sets of accessible information, and in effect they are generally different. With multiple reflections, the number of different projections $e_{\mathbf{h}}$ of ε becomes larger, and ε^M obtained from multiple reflections is expected to be closer to $\langle \varepsilon \rangle$ than those obtained from individual reflections.

In order to apply the above formalism to experimental data, two features of actual measurements must be taken into consideration. First, a typical X-ray measurement does not cover the complete hemisphere but only a part of it. Therefore, the integrals in the ε^M -defining formulas (10)–(13) and (24) must be modified. Instead of integrating over the whole sphere, the region of integration must be limited to the intersection of the experimentally accessible domains of the pole figures $p_{\mathbf{h}}$ and $e_{\mathbf{h}}$. Second, the experimental data are not continuous but discrete, *i.e.* one actually has some discretely distributed $e_{\mathbf{h}}(\mathbf{l}^n)$ and $p_{\mathbf{h}}(\mathbf{l}^n)$ ($n = 1, \dots, N$) instead of continuous $e_{\mathbf{h}}(\mathbf{l})$ and $p_{\mathbf{h}}(\mathbf{l})$. One can deal with such data by standard techniques of texture analysis, *e.g.* by expansion into spherical harmonics (Bunge, 1982), or using the ‘direct’ method with the integrals over \mathbf{l} replaced by sums over n , and with $p_{\mathbf{h}}(\mathbf{l}^n)$ incorporating the spherical area represented by \mathbf{l}^n . In relation to the latter approach, one should be warned of the idea that ‘one is absolutely free in choosing the φ, ψ pairs (measurement directions)’ (Ortner, 2009); with the discrete approach and spherical areas ignored, a non-uniform density of measurement directions will act like an artificial non-uniform intensity pole figure, and it may bias the resulting ε^M .

Note here that the expression for ε^M does not involve the orientation density function f . With an incomplete pole figure p , the pole figure normalization factor in expressions for A^C and ε in equations (13) would not be known, but it is the same in both cases and cancels out when ε^M is calculated. However, this does not occur if multiple incomplete pole figures $p_{\mathbf{h}}$ and equations (24) are used. In practice, the normalization coefficients can be estimated on the basis of the range of ψ angle, and having slightly inaccurate normalization coefficients implies slightly different contributions of particular pole figures to ε^M . The orientation density function f is necessary only if accurate normalization coefficients of the incomplete pole figures are needed.

6. Examples

To assess the method’s performance, it is applied to some particular cases. The first subsection concerns special textures: uniform orientation distribution and an infinitely sharp texture corresponding to a single crystal. An application to some simulated data is given in the second subsection.

6.1. Special textures

6.1.1. Uniform orientation distribution. The uniform distribution of orientations [$f(g) = 1$] implies a uniform distribution of directions [$p(\mathbf{l}) = 1$]. If vectors \mathbf{l} are uniformly distributed over the complete sphere, A^C is given by

$$A_{ijkl}^C = \int_{\mathbf{l}} l_i l_j l_k l_l = \frac{1}{15} (\delta_{ij}\delta_{kl} + 2I_{ijkl}^{(4)}), \quad (25)$$

or using the abbreviation **iso** defined by Morawiec (1994), it can be expressed as $A^C = \mathbf{iso}(1/3, 2/15)$. Hence, its inverse A^S equals $\mathbf{iso}(3, 15/2)$, or explicitly

$$A_{ijkl}^S = \frac{3}{2} (5I_{ijkl}^{(4)} - \delta_{ij}\delta_{kl}). \quad (26)$$

With $\varepsilon_{ij} = \int_{\mathbf{l}} e(\mathbf{l}) l_i l_j$, one gets

$$\varepsilon_{ij}^M = \frac{3}{2} \int_{\mathbf{l}} e(\mathbf{l}) (5l_i l_j - \delta_{ij}). \quad (27)$$

If multiple strain pole figures $e_{\mathbf{h}}$ are used, $e(\mathbf{l})$ must be replaced by the arithmetic average of $e_{\mathbf{h}}(\mathbf{l})$. This is the explicit continuous form of the discrete solution of Winholtz & Cohen (1988), listed as equation (9) in that article.

6.1.2. Single-component infinitely sharp texture. For simplicity, let the crystal symmetry be C_{2h} ($2/m$), and let \mathbf{h} be perpendicular to the symmetry axis (this is to have even pole figures and to avoid discussing the complication described in §4). Let the ODF have just two infinitely high peaks at $g = g^0$ and the symmetrically equivalent orientation cg^0 , and a negligible but nonzero background [in order to have $p(\mathbf{l}) \neq 0$ obeyed]. The intensity pole figure p of the type $\mathbf{h} \propto \mathbf{l}^c$ has infinitely high peaks at $\mathbf{l} = \pm\mathbf{l}^0$, where $l_i^0 = g_{ij}^0 l_j^c$. The strain pole figure e is reliably determinable only at $\mathbf{l} = \pm\mathbf{l}^0$. With such p and e , the formulae (13) give

$$A_{ijkl}^C = l_i^0 l_j^0 l_k^0 l_l^0 \quad \text{and} \quad \varepsilon_{ij} = e(\mathbf{l}^0) l_i^0 l_j^0. \quad (28)$$

The above A^C is singular, and its pseudoinverse equals A^C , *i.e.* $A^S = A^C$. Hence, the strain tensor ε^M calculated using equation (14) is

$$\varepsilon_{ij}^M = e(\mathbf{l}^0) l_i^0 l_j^0. \quad (29)$$

This result has a simple interpretation: In directions \mathbf{l} inclined to \mathbf{l}^0 by an angle ξ , the estimated strain $\varepsilon_{ij}^M l_i l_j$ equals $e(\mathbf{l}^0) \cos^2 \xi$. Thus, even though the strain data are limited to the single point \mathbf{l}^0 , the strain $\varepsilon_{ij}^M l_i l_j$ agrees with the measurement result at that point [$\varepsilon_{ij}^M l_i^0 l_j^0 = e(\mathbf{l}^0)$], and it vanishes in directions perpendicular to \mathbf{l}^0 .

The comparison of the two extreme cases considered in §§6.1.1 and 6.1.2 shows the impact of texture. If the weighting by the intensity pole figure were ignored and the uniform ODF was assumed when the actual texture has an infinitely sharp component, the tensor ε^M resulting from equation (27) for data restricted to $e(\mathbf{l}^0)$ would be determined by the unreliable shape of $e(\mathbf{l})$ for \mathbf{l} other than $\pm\mathbf{l}^0$.

6.2. Example texture of moderate sharpness

This section shows the results of application of the described method to a more realistic model. The model is based on an assumed orientation density function $f = f(g)$ and a strain function $\varepsilon = \varepsilon(g)$. The example illustrates the level of ambiguity in determination of the average strain in the case of a relatively weak texture. It also demonstrates how the deviation between the calculated and average strain tensors is affected by the use of multiple pole figures and by the incompleteness and discreteness of pole figure data. The results are not affected by any experimental errors.

6.2.1. Model. The explicit expression for the model ODF shown in Fig. 1 is

$$f(g) = 0.12291237 \left\{ \sum_{i,j} \exp[12 \text{Tr}(c_i g_0 s_j g^T)] / 10^{14} + 1 \right\}, \quad (30)$$

where $g_0 = \Phi[\text{arcsec}(5^{1/2}), \arccos(2/3), \text{arcsec}(5^{1/2})]$, and the sum is over the (24) cubic crystal and (4) orthorhombic sample symmetry operations c_i and s_j , respectively. (Because of the specific choice of g_0 , the sample symmetry with respect to orientations is cubic.) In the parlance of texture analysis, the ODF consists of a single component at $\{2\bar{1}2\}\langle 22\bar{1}\rangle$, with the peak modeled by a symmetric von Mises–Fisher distribution (Morawiec, 2004). This function is similar to the Santa Fe model of Matthies (1988), which is known to have nonzero odd coefficients in the expansion into generalized spherical harmonics, and in consequence, some unreduced intensity pole figures have nonzero odd components. The model of the strain field is given by

$$\varepsilon(g) = g^T \text{map}[a, g \varepsilon_0 g^T] g, \quad (31)$$

where $\varepsilon_0 = \text{diag}[5, -4, -1]$ (in arbitrary units, e.g. in 10^{-4}), $a(x) = \text{sgn}(x) \ln(1 + |x|)$ is an attenuation function of a real variable and $\text{map}[a, X]$ denotes the matrix obtained by application of a to each entry of X . Both f and ε are symmetric with respect to the crystal symmetry, i.e. $f(cg) = f(g)$ and $\varepsilon(cg) = \varepsilon(g)$. With s being a proper rotation of the specimen

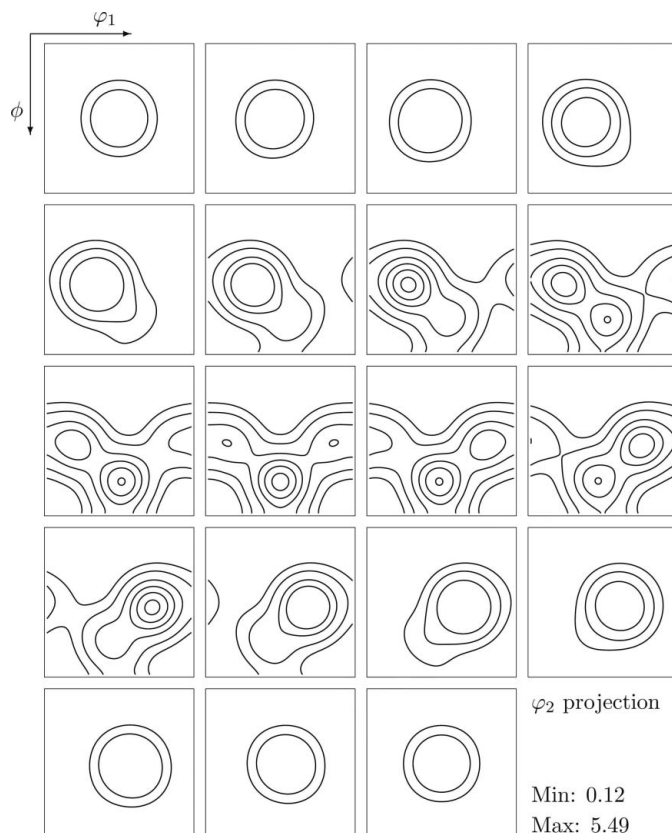


Figure 1
Model orientation density function. The isolines are 0.5, 1.0, 2.0, 3.0, 4.0 and 5.0.

symmetry group, one has $f(gs) = f(g)$ and $\varepsilon(gs) = s \varepsilon(g) s^T$. The functions f and ε give the average strain tensor

$$\langle \varepsilon \rangle = \int_g f(g) \varepsilon(g) = \text{diag}[2.405, -1.940, -0.515]. \quad (32)$$

The non-diagonal entries of the above tensor and the ε^M tensors below are all 0.000.

6.2.2. Results. The complete $\{110\}$ intensity pole figure (calculated from the model ODF) and the $\{110\}$ strain pole figure (calculated from the model ODF and the model strain field) are shown in Figs. 2 and 3, respectively. The tensor obtained by application of equation (14) to this pair of complete pole figures equals

$$\varepsilon^M = \text{diag}[2.389, -1.928, -0.511]. \quad (33)$$

The magnitude $\|\varepsilon^d\|$ of the inaccessible part ε^d of the actual ε^t for the $\{110\}$ reflection is shown in Fig. 4. It takes its largest values at the rim of the figure, where the strain pole figure has extrema. The magnitude of the deviation between ε^M and the actual $\langle \varepsilon \rangle$ is $\|\langle \varepsilon \rangle - \varepsilon^M\| = \|\int_{\mathbf{l}} p(\mathbf{l}) \varepsilon^d(\mathbf{l})\| = 0.021$. The calculations were also carried out for discrete data from incomplete pole figures. With the $\{110\}$ pole figures given on the grid of directions shown in Fig. 5, one gets

$$\varepsilon^M = \text{diag}[2.354, -1.859, -0.520]. \quad (34)$$

The other pairs of pole figures used in this example are $\{100\}$, $\{111\}$ and $\{311\}$. The relative deviations $\Delta = \|\langle \varepsilon \rangle - \varepsilon^M\| / \|\langle \varepsilon \rangle\|$ between $\langle \varepsilon \rangle$ and ε^M obtained from individual pairs of intensity and strain pole figures are collected in Table 1. The deviation is to some extent linked to the multiplicity of the reflection. [Here, it is the number of the proper crystal point

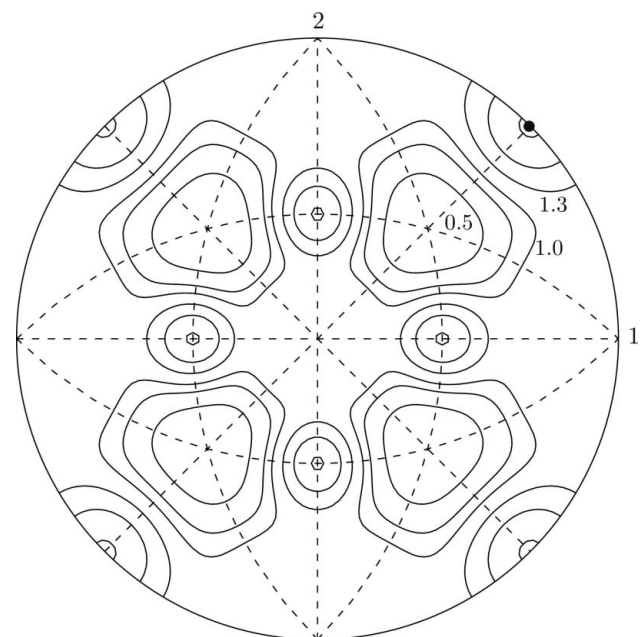


Figure 2
The $\{110\}$ intensity pole figure calculated from the orientation density function shown in Fig. 1. The minimal and maximal values are 0.22 and 1.92, respectively, and the isolines are 0.5, 0.8, 1.0, 1.3, 1.6 and 1.9. The filled black circle marks one of the maxima.

group operations that leave $\pm\mathbf{h}$ unchanged. The multiplicities of {100}, {110}, {111} and {311} are 8, 4, 6 and 2, respectively.] The larger the multiplicity, the smaller the number of distinct integration paths (determined by fixed \mathbf{l} and varying γ), and the larger the deviation.

With four pairs of complete pole figures {100}, {110}, {111} and {311} used together, equations (24) give

$$\varepsilon^M = \text{diag}[2.411, -1.944, -0.516], \quad (35)$$

deviating from the average strain tensor $\langle\varepsilon\rangle$ by $\Delta = 0.002$. Similarly, the discrete data of four pairs of incomplete pole figures (each given on the grid shown in Fig. 5) lead to

$$\varepsilon^M = \text{diag}[2.409, -1.959, -0.511], \quad (36)$$

which deviates from the average strain tensor by $\Delta = 0.006$. The simultaneous use of four pairs of pole figures gives the deviation Δ reduced roughly by an order of magnitude compared to the average of deviations for individual pairs. In

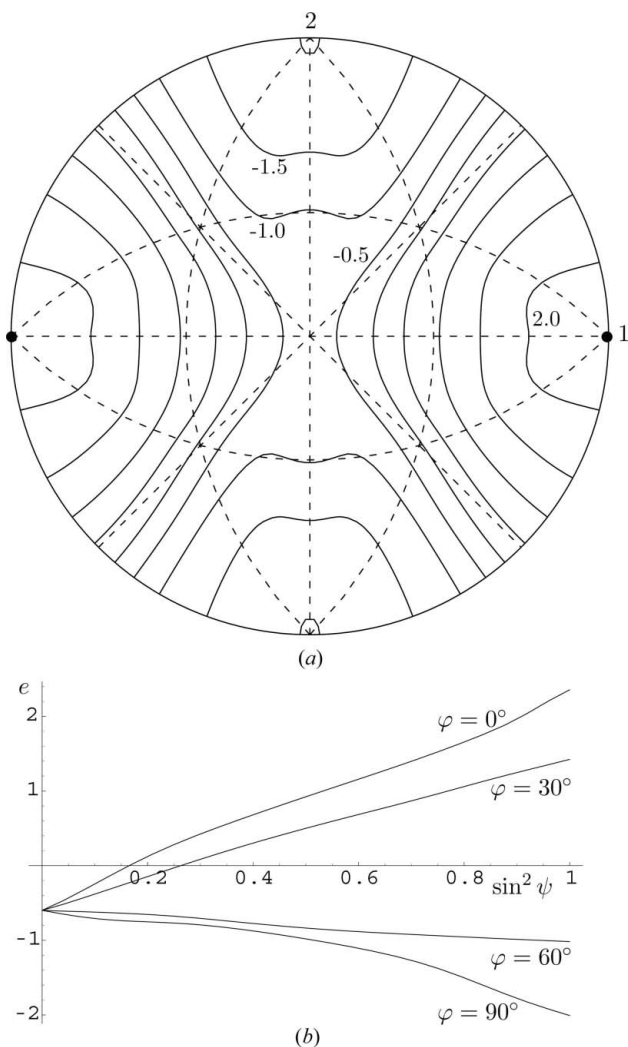


Figure 3
(a) The {110} strain pole figure calculated from the model strain function $\varepsilon = \varepsilon(g)$ and ODF shown in Fig. 1. The minimal and maximal values are -2.01 and 2.36 , respectively, and the isolines are $0, \pm 0.5, \pm 1.0, \pm 1.5$ and ± 2.0 . Filled black circles mark the maxima. (b) Some $\sin^2 \psi$ plots for the {110} reflection.

all cases, the incompleteness of data has a significant impact on the results because, in the considered model, the principal

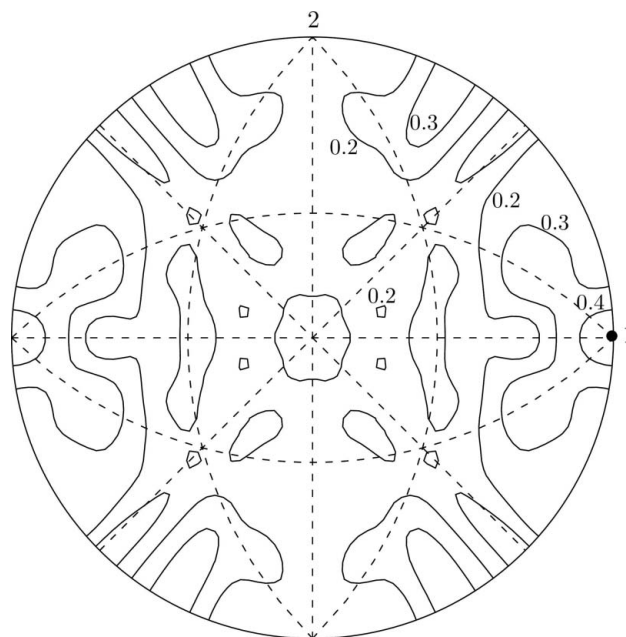


Figure 4
The magnitude $\|\varepsilon^d\|$ of the deviation between the actual ε^l and ε^m for the reflection {110}. The unlabeled isolines correspond to 0.1. The filled black circle marks the maximum of 0.45.

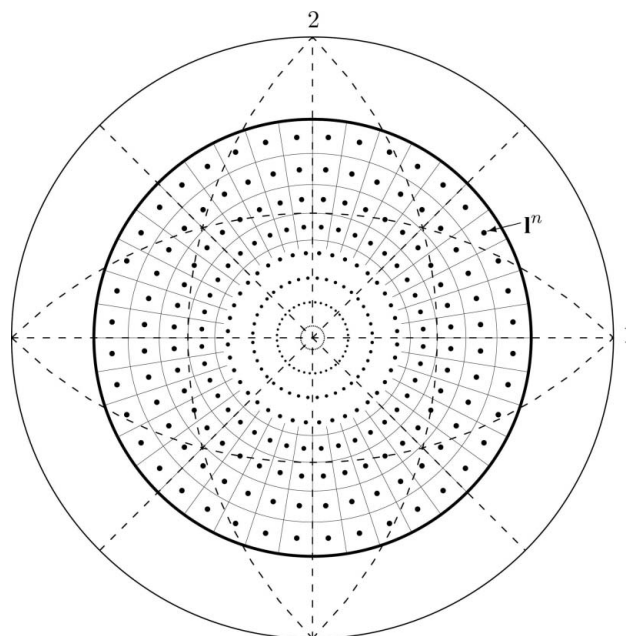


Figure 5
The grid of directions \mathbf{l}^n on an incomplete pole figure. The spherical angles of neighboring vectors differ by 9° in ψ or φ . Each \mathbf{l}^n represents a $9 \times 9^\circ$ cell in the domain $\psi \times \varphi$. The spherical area of the cell is $(\pi/10) \sin(\pi/40) \sin \psi_n$, where ψ_n is the polar angle of \mathbf{l}^n . For clarity, only high- ψ cells are drawn. From the viewpoint of spherical geometry the vectors are close to but not exactly at the centers of the cells. With high (low) density of nodes at small (large) ψ , the grid is clearly not optimal, but it refers to conventional measurement strategies (steps in ψ for fixed φ).

Table 1

The deviation Δ between $\langle \varepsilon \rangle$ and ε^M obtained from individual pairs of intensity and strain pole figures.

| Type of pole figures | {100} | {110} | {111} | {311} |
|----------------------|-------|-------|-------|-------|
| Complete | 0.049 | 0.007 | 0.015 | 0.007 |
| Incomplete, discrete | 0.084 | 0.031 | 0.074 | 0.024 |

information is concentrated at the rim of the strain pole figures (*cf.* Fig. 3).

7. Final remarks

The paper describes a method of processing strains obtained by determination of Bragg peak positions to get a constant tensor best representing the average strain in textured polycrystalline materials. The input data are intensity pole figures and strain pole figures. The procedure is a generalization of that of Winholtz & Cohen (1988), and it is an alternative to stress determination schemes stemming from the original $\sin^2 \psi$ method. The $\sin^2 \psi$ -based approaches require fewer data, but there is no clear relationship between their results and the actual average stresses. The link between the result ε^M of the presented procedure and $\langle \varepsilon \rangle$ is more explicit. However, despite the use of a general fitting method, the resulting tensor ε^M is generally different from the average strain tensor $\langle \varepsilon \rangle$. The level of discrepancy depends on the quantity of measurement data, specifically, the number and range of pole figures, and on the multiplicity of the corresponding reflections.

There is an additional complication caused by evenness of experimental pole figures: generally, the difference between ε^M and $\langle \varepsilon \rangle$ is increased by a term involving experimentally inaccessible odd parts of pole figures. With sufficiently high crystal symmetry, this issue is concealed if the used reflection \mathbf{h} is equivalent to $-\mathbf{h}$ by a symmetry operation being a proper rotation.

Clearly, the proposed formalism can also be applied to data intended for simpler methods, *e.g.* the Dölle–Hauk method (Hauk, 1997). It is enough to read these data as a strain pole figure given on an ill-adapted grid, and to account for spherical areas represented by particular grid points.

Note that strain pole figures can be used to estimate the complete strain field $\varepsilon = \varepsilon(g)$ (Behnken, 2000; Schuren *et al.*, 2012; McNelis *et al.*, 2013), and hence the average strain tensor can be obtained. This procedure, however, would be more complex than that described above, and such a detour would be additionally affected by ambiguities arising in strain-field estimation (Van Houtte & De Buyser, 1993) or by constraints imposed to eliminate them.

The new procedure is described in detail, but some related issues have not been addressed. In particular, having a given data set, it would be interesting to know how to get the actual range of the indeterminable part of $\langle \varepsilon \rangle$ (or the strains ε^d). Another issue is how to estimate the impact of inaccessibility of the odd parts of pole figures. These essentially mathematical problems are beyond the scope of this paper. Also the subject

of getting average stress tensors from estimated average strain tensors and the problem of determining effective elastic constants are ignored. They are extensively discussed elsewhere (see *e.g.* Beran & McCoy, 1970; Kröner, 1986; Morawiec, 1994; and references therein).

APPENDIX A

Orientation matrix and Euler angles convention

A crystallite orientation is described by a special orthogonal matrix g transforming vector components given in the Cartesian specimen reference system to the Cartesian crystal reference system. The Euler angles $\varphi_1, \phi, \varphi_2$ determining the orientation are related to the matrix g via

$$g = \Phi(\varphi_1, \phi, \varphi_2) = \begin{bmatrix} c_1 c_2 - s_1 s_2 c_0 & s_1 c_2 + c_1 s_2 c_0 & s_2 s_0 \\ -c_1 s_2 - s_1 c_2 c_0 & -s_1 s_2 + c_1 c_2 c_0 & c_2 s_0 \\ s_1 s_0 & -c_1 s_0 & c_0 \end{bmatrix}, \quad (37)$$

where $s_i = \sin \varphi_i$, $c_i = \cos \varphi_i$, $s_0 = \sin \phi$ and $c_0 = \cos \phi$. For more on this and other orientation parameterizations used in texture analysis, see Bunge (1982) and Morawiec (2004).

References

- Behnken, H. (2000). *Phys. Status Solidi (A)*, **177**, 401–418.
- Ben-Israel, A. & Greville, T. N. E. (2003). *Generalized Inverses. Theory and Applications*. New York: Springer.
- Beran, M. J. & McCoy, J. J. (1970). *Int. J. Solids Struct.* **6**, 1035–1054.
- Bollenrath, B., Hauk, V. & Müller, E. H. (1967). *Z. Metallkd.* **58**, 76–82.
- Bunge, H. J. (1982). *Texture Analysis in Materials Science*. London: Butterworth.
- Dölle, H. (1979). *J. Appl. Cryst.* **12**, 489–501.
- Hauk, V. (1997). *Structural and Residual Stress Analysis by Nondestructive Methods*. Amsterdam: Elsevier Science BV.
- Kröner, E. (1986). *Modelling Small Deformations of Polycrystals*, edited by J. Gittus & J. Zarka, ch. 8, pp. 229–291. New York: Elsevier Applied Science Publishers.
- Larsson, C., Clausen, B., Holden, T. M. & Bourke, M. A. M. (2004). *Scr. Mater.* **51**, 571–575.
- Leeuwen, M. van, Kamminga, J. D. & Mittemeijer, E. J. (1999). *J. Appl. Phys.* **86**, 1904–1914.
- Leoni, M., Welzel, U., Lamparter, P., Mittemeijer, E. J. & Kamminga, J. D. (2001). *Philos. Mag. A*, **81**, 597–623.
- Liu, C. Q., Li, W. L. & Fei, W. D. (2010). *Acta Mater.* **58**, 5393–5401.
- Macherauch, E. (1966). *Exp. Mech.* **6**, 140–153.
- Matthies, S. (1979). *Phys. Status Solidi (B)*, **92**, K135–K138.
- Matthies, S. (1988). *ICOTOM, Eight International Conference on Textures of Materials*, edited by J. S. Kallend & G. Gottstein, pp. 37–48. Warrendale: The Metallurgical Society.
- Matthies, S. & Wenk, H. R. (1985). *Preferred Orientation in Deformed Metals and Rocks. An Introduction to Modern Texture Analysis*, edited by H. R. Wenk, pp. 139–147. Orlando: Academic Press.
- Maurer, G., Neff, H., Scholtes, B. & Macherauch, E. (1988). *Textures Microstruct.* **8–9**, 639–678.
- McNelis, K. P., Dawson, P. R. & Miller, M. P. (2013). *J. Mech. Phys. Solids*, **61**, 428–449.
- Morawiec, A. (1994). *Textures Microstruct.* **22**, 139–167.

- Morawiec, A. (2004). *Orientations and Rotations. Computations in Crystallographic Textures*. Berlin: Springer.
- Morawiec, A. & Pospiech, J. (1989). *Textures Microstruct.* **10**, 243–264.
- Noyan, I. C. & Cohen, J. B. (1987). *Residual Stress. Measurement by Diffraction and Interpretation*. New York: Springer.
- Ortner, B. (2008). *Int. J. Mater. Res.* **99**, 933–941.
- Ortner, B. (2009). *Adv. X-ray Anal.* **52**, 763–772.
- Pang, J. W. L., Rogge, R. B. & Donaberger, R. L. (2006). *Mater. Sci. Eng. A*, **437**, 21–25.
- Perlovich, Yu., Bunge, H. J. & Isaenkova, M. (1997). *Textures Microstruct.* **29**, 241–266.
- Schuren, J. C., Miller, M. P. & Kazimirov, A. (2012). *Exp. Mech.* **52**, 461–479.
- Van Houtte, P. & De Buyser, L. (1993). *Acta Metall. Mater.* **41**, 323–336.
- Wielewski, E., Boyce, D. E., Park, J. S., Miller, M. P. & Dawson, P. R. (2017). *Acta Mater.* **126**, 469–480.
- Winholtz, R. A. & Cohen, J. B. (1988). *Aust. J. Phys.* **41**, 189–199.
- Wit, R. de (1997). *J. Appl. Cryst.* **30**, 510–511.